Analytical methods for dynamic-response of underground structures.

Ayumi KUROSE[1−2], Pierre BEREST[1], Benoît BROUARD[1−2]

[1]Laboratoire de Mécanique des Solides, CNRS UMR 7649, Ecole polytechnique, Palaiseau.
[2]Brouard Consulting, 101 rue du Temple, 75003 Paris.

Résumé : *A dynamic response-analysis methodology of deep underground structures is proposed by means of an analytical method. Damage observed during some recent earthquakes call into question the allowable damage level for an underground structure. A simple and realistic model of an underground linear structure is an infinite, linear, unlined or lined cavity with circular cross-section in an unbounded, elastic, homogeneous and isotropic medium. Through the response analysis under monochromatic or earthquake loadings, this paper shows a comparison study between computation and in-situ measurements, how to develop a response spectrum and to study the structure stability, to finally give some earthquake-resistant design methods of underground structures.*

1 Introduction

For underground works in seismic zones, or such strategic facilities as underground hydrocarbon storage or high-level radioactive waste disposal, that require earthquake design, calculation methods and regulation codes must be developed as rigorously as in the case of surface structures. Damage observed during some recent earthquakes of magnitude higher than 6.5, such as the 1995 Hyogo-ken Nanbu earthquake in Japan, call into question the allowable damage level for an underground structure.

Observations of damage — Generally, damage is localized at four zones having a particular geological or structural type — namely, (i) fault-crossing zones, (ii) joint zones between geometrically or mechanically different properties, (iii) zones of low overburden, and (iv) zones of great overburden in weak areas. In general, tunnels with large overburden are located in hard rock, and low seismic effects are expected. Yet, during excavation, such tunnels can encounter some altered or faulted zones that are weaker than the surrounding rock mass. For these tunnels, the earthquake-related damage is located within these weak zones as in the case of the Rokkoh tunnel, in Kobe, Japan [Sakurai, 1995]. The Rokkoh tunnel is 16-kilometer long and crosses the mountainous region between Osaka and Okayama. Several tunnel sections have an overburden of several hundred meters. During excavation, several fault zones were encountered. Damage during the 1995 Hyogo-ken Nanbu earthquake is localized at the fault zones and are certainly due to large deformations of the vertical cross-section, which cause cracking, crushing, falling of the concrete lining, bending of reinforcing bars and rising of the invert. From observations of damaged underground structures described in the literature, several authors carried out statistical studies to correlate the damage level with various seismological parameters, such as magnitude, seismic intensity, epicentral distance or maximum acceleration at ground surface : [Duke and Leeds, 1959], [Dowding and Rozen, 1978], [Dowding, 1979], [Owen and Scholl, 1979] (127 damage cases), [Clure, 1982], [Sharma and W.R., 1991] (192 cases), [Martin and Godefroy, 1991], [Power et al., 1998]. In the last reference, the authors provide rigorous criteria for the choice of earthquake damage data and only use well-documented data related to dynamic loadings during earthquakes of moment-magnitude higher than 6.6. As a whole, 204 cases are considered, 97 of which come from the 1995 Hyogo-ken Nanbu (Japan) earthquake, 31 from the 1994 Northridge (California, USA) earthquake and 22 from the 1989 Loma Prieta (California, USA) earthquake. Power et al. also present available earthquake-resistant design techniques. Observations and statistical analyses indicate zones in which damage to underground

structures is concentrated and enable determination of relevant seismological, geological and structural parameters for the earthquake-design of structures. The seismological parameters are linked by the attenuation laws and are mainly those that give the size of earthquakes and their influence on a given site — namely : magnitude, epicentral distance and peak ground acceleration. For the geological parameters, Sharma and Judd [Sharma and W.R., 1991] attempt to correlate the damage level and the nature of the ground, but the lack of data makes their study difficult. The structural parameters concern structure size, structural properties, lining and depth. Most of these parameters were proposed by Martin and Godefroy [Martin and Godefroy, 1991].

The limitations of current earthquake-design methods for deep structures — The damage observed after large earthquakes and response analysis show the vulnerability of the vertical cross-section of underground works. With regard to the evaluation of earthquake-related mechanical effects in the cross-section, current earthquake-resistant design standards only suggest methods for structures constructed in a soil laying over a rigid basement to which a horizontal acceleration is applied. The following three criticisms can be made against this rigid-basement model : (i) this model cannot be applied to a structure constructed in a thick homogeneous rock mass, as is often the case when an underground hydrocarbon-storage facility or a nuclear waste-disposal site are considered. At the Kamaishi Mine in a granitic environment, a basement cannot be identified ; (ii) the model gives a preeminent role to the vibration modes of the overburden layer, an often artificial notion ; (iii) the calculation of seismic effects on the underground works by the rigid-basement model often uses time-consuming finite-element methods. Some authors propose failure mechanisms to interpret damage to tunnels with low or high overburden (Types 3 and 4 of above-described damage cases) observed during the 1995 Hyogo-ken Nanbu earthquake. Asakura et al. [Asakura et al., 1998] suggest using static seismic-deformation methods to calculate the stress in the lining. If static methods are relevant for shallow structures, as recommended by the Japanese regulation codes, they are unsuitable for deep structures and insufficient to understand the frequency dependence of structural response and damage modes. Thus, the dynamic analysis carried out by Uenishi et al. to explain the damage modes of deep tunnels, such as is observed in the Rokkoh tunnel is very interesting [Uenishi et al., 1999]. In this study, the tunnel is assimilated to a cylindrical lined cavity with circular cross-section excavated in an infinite, elastic, linear, homogeneous and isotropic medium through which sinusoidal P-waves propagate. These mechanical assumptions seem to be suitable for the response analysis of deep underground structures. Uenishi's idea is extended in a larger context in [Kurose, 2000] and presented below.

2 A new dynamic analysis of deep underground structures

The model considered here is an infinite, linear, unlined or lined cavity with circular cross-section of radius a in an unbounded, elastic, homogeneous and isotropic medium characterized by the Poisson's ratio, ν, density, ρ, undamped and complex velocities for S- and P-waves, c_{s0}, c_{p0}, c_s, c_p and damping ratios, ζ_s and ζ_p with $c_s = c_{s0}\sqrt{1 + 2i\zeta_s}$ and $c_p = c_{p0}\sqrt{1 + 2i\zeta_p}$. Let assume $\zeta_s = \zeta_p$. The ratio between c_p and c_s, is a function of Poisson's ratio, noted κ, defined by

$$\kappa(\nu) = \sqrt{2(1-\nu)/(1-2\nu)} = c_p/c_s = \beta/\alpha \tag{1}$$

where $\alpha = \omega/c_p$ is the compressional wave number, $\beta = \omega/c_s$ is the shear wave number, and ω is the circular frequency.

The following studies use cylindrical coordinates (r, θ, z), which are related to the Cartesian coordinates (x, y, z) by $x = r\cos\theta$, $y = r\sin\theta$, $z = z$, by orienting the z-axis in the longitudinal direction of the structure (Fig.1). Thus, the (r, θ)- or (x, y)-plane represents the plane of the structure's cross-section. The structure is subjected to an incident plane wave that propagates upward ($x > 0$) and

whose incident angle is φ_w. A cavity of radius a is imlined or has a lining or an elastic or fluid inclusion which is in perfect contact with the surrounding medium.
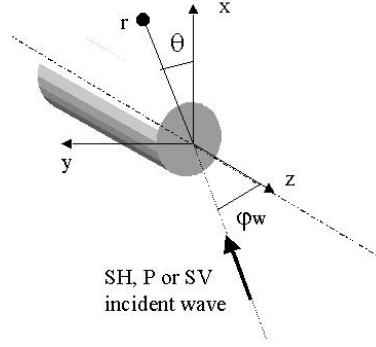

FIG. 1 – Model type used for underground structures in the proposed methodology

The mechanical calculation for an infinite cylindrical cavity is simpler than that for a cavity of finite length. A response analysis of finite and infinite cavities to impulsive loading has been carried out by Nogami and Zhu [Nogami and Zhu, 1994] ; it shows that the maximum stress induced around an infinite cavity is greater than the stress around an finite cavity. Thus, the calculation for infinite structures is conservative from an earthquake-resistant viewpoint.

A wave number, γ, is introduced to express Snell's law in the theory of wave propagation :

$$\gamma = \alpha \cos \varphi_p = \beta \cos \varphi_s \tag{2}$$

where angles φ_p and φ_s are associated to the P- and S-waves. Equation (2) expresses the conservation along the wave path of the *ray parameter*, noted as $p = \cos \varphi_p / c_p = \cos \varphi_s / c_s$. Then, wave numbers α_w and β_w are defined by

$$\alpha_w^2 \quad = \alpha^2 - \gamma^2 = \alpha^2 \sin^2 \varphi_p \quad = \beta^2 \left(1/\kappa^2(\nu) - \cos^2 \varphi_s \right) \tag{3}$$

$$\beta_w^2 \quad = \beta^2 - \gamma^2 = \beta^2 \sin^2 \varphi_s \quad = \alpha^2 \left(\kappa^2(\nu) - \cos^2 \varphi_p \right) \tag{4}$$

In frequency domain, the general expressions of stress and displacement induced in the lining and the rock mass are, in cylindrical coordinates, of the form :

$$\sigma_{ij}^h \quad = \quad \rho_h c_{sh} v_0(\omega) \mu_{ij}^{hw}(\varphi_w, \nu_h, \beta_h a, \beta_h r, \theta) \exp(i\gamma z) \tag{5}$$

$$u_i^h \quad = \quad u_0(\omega) \pi_i^{hw}(\varphi_w, \nu_h, \beta_h a, \beta_h r, \theta) \exp(i\gamma z) \tag{6}$$

where $w = p$, sv or sh, as a function of wave type ; $h = m$ or l, if the stress is obtained in the rock mass or the lining ; ρ_h, c_{sh}, ν_h : bulk density, shear wave velocity, Poisson's ratio ; $v_0(\omega)$: velocity in frequency domain ; μ_{ij}^{hw} : the dimensionless function corresponding to the ijth-component of the stress tensor, and π_i^{hw} : the dimensionless function corresponding to the ith-component of the displacement, given in Appendix A ; φ_w : incident angle ; $\beta_h = a/c_{sh}$: shear wave number ; (r, θ, z) : cylindrical co-ordinates. The introduction of velocity, v_0 in stress formula (5), instead of displacement or acceleration, has two advantages : (i) the product $\rho c_s v_0$ represents the maximum stress in the free field induced by the wave propagation in the medium — that is, the presence of the cavity introduces a multiplying factor,

$\underline{\underline{\mu}}$, in the expression of stress; and (ii) when using actual earthquake data, it avoids several time integrations of earthquake motion usually recorded as acceleration or velocity; those integrations introduce additional errors. The inverse Fourier transformation of stress and displacement components obtained by Eqs.(5) and (6) yields the time-dependent values of mechanical fields. The maximum shear stress, τ_{max} and the corresponding normal stress, σ_n, can be calculated from the time-dependent stress tensor. From the perspective of structural stability, the worst situation is when the principal stress directions of the dynamic stress tensor coincide with those of the static stress tensor. In this case, the total maximum shear, as well as the corresponding total normal stress, is the sum of the dynamic and static quantities, which is why the study of dynamic shear stress is relevant to this approach. For SH-incidence, the dynamic non-zero stress component at the traction-free cavity wall is $\sigma_{\theta z}$, the maximum shear is $|\sigma_{\theta z}|$ and the normal stress is nil; for P- and SV-incidences, the dynamic non-zero stress component is $\sigma_{\theta\theta}$, the maximum shear is $|\sigma_{\theta\theta}|/2$ and the normal stress is $\pm|\sigma_{\theta\theta}|/2$.

The stress-response spectrum, SRS, is defined as the maximum value of τ_{max} during the loading time :

$$SRS = \max_t \{\tau_{max}\} \tag{7}$$

The characteristic period of structure is defined as $T_c = a/c_s$. The usual values of T_c for the existing structures are between 0.0001 (usual tunnel) and 0.01 second (underground oil storage). For any dynamic loading, definition (7) of the stress-response spectrum yields :

$$SRS(\rho, \nu, c_s, T_c) = \max_{t,\theta\in[0,2\pi]} \{\tau_{max}(\rho, \nu, c_s, T_c, \theta, t)\} = \rho c_s v_0 \{\mu_{SRS}(\nu, T_c)\} \tag{8}$$

This formula shows that, if the site is fixed, ρ, ν and c_s are given, and the SRS values depend only on T_c.

3 Response of unlined cavity under monochromatic plane waves

The problem of monochromatic-wave diffraction by unlined cavities in infinite, elastic linear, homogeneous and isotropic media is fully studied by Mow and Pao [Pao and Mow, 1973]. This section presents some complementary results for the dynamic-response-analysis interest. The incident wave propagates with an angle, $\varphi_w \in [0^o, 90^o]$, related to the tunnel axis (see Fig.1). If $\underline{k}$ is the wave-number vector, the velocity of the incident plane wave is of the form :

$$\underline{v}_0 = v_0 \exp[i(\underline{k}.\underline{r} - \omega t)]\underline{e}_w \tag{9}$$

where $\underline{e}_w$ is the unit vector in the direction of the incident displacement.

Different incident waves induce different structure responses, and some cases generate larger stress amplitudes around a cavity than others. Thus, it is possible to determine the most unfavorable wave inputs from the viewpoint of dynamic response. The P-wave amplitudes are usually lower than S-wave amplitudes. Thus, the discussion is mainly carried out for SH- and SV-incidence. The SH-movement is perpendicular to the plane of the cross-section and the SV- movements are done in the plane of the cross-section The following incidence cases are handled : (i) vertical incidence of the superposition of SH and SV waves; (ii) incidence with $\varphi_w \leq 90^o$.

First, the responses of cavities subjected to vertical-incident waves obtained by the superimposition of SV- and SH-waves are analyzed. SH- and SV-movements are assumed to be oriented by unit vectors $\underline{e}_z$ and $\underline{e}_y$, respectively. With the assumption that SV- and SH-waves are in phase, definition (9) of the incident velocity is modified to be :

$$\underline{v}_0 = v_0 \exp[i(\beta x - \omega t)][\cos(\theta_v)\underline{e}_z + \sin(\theta_v)\underline{e}_y] \tag{10}$$

in which $\theta_v \in [0, 90^o]$. Cases $\theta_v = 0^o$ and $\theta_v = 90^o$ correspond, respectively, to SV- and SH-incidences. Fig.2 shows the maximum values of $|\mu_{shv}| = SRS/(\rho c_s |v_0|)$ as functions of θ_v and T_c ($\nu = 0, 15, f_0 = 10$ Hz). The peak values are of about 2.35, obtained when $T_c f_0 = 0.08$ and for case $\theta_v = 0^o$ — i.e., for SV-incidence. Those values slightly decrease with Poisson's ratio ; the peak value is 2.2, for $\nu = 0.35$) [Pao and Mow, 1973].

Using SV-incidences, the stresses are evaluated for different values of incident angle $\varphi_w \in [0, 90^o]$. In Fig.3, the maximum value of $|\mu_{qcq}|$ at the wall is shown as a function of incident angle φ_w and T_c, for Poisson's ratio of $\nu = 0.15$ and frequency $f_0 = 10$ Hz. For any T_c, the values increase with the incident angle and maximum stresses occur for $\varphi_w = 90^o$ — i.e., for vertical incidence.
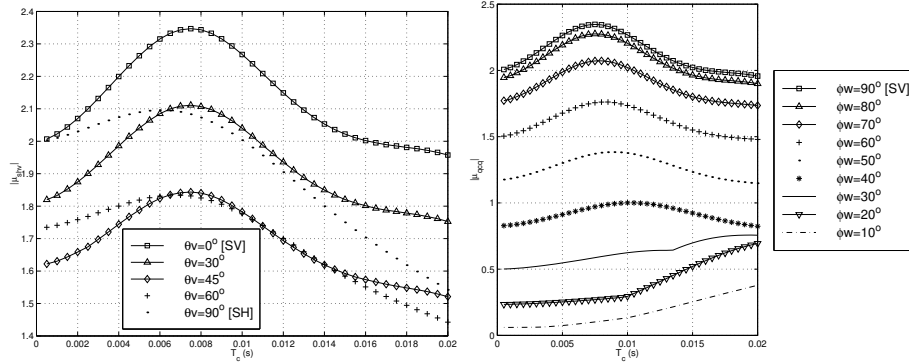

FIG. 2 – Left - Maximum values of $|\mu_{shv}|$ as a function of T_c ($\nu = 0.15$, $f_0 = 10$ Hz)

FIG. 3 – Right - Maximum values of $|\mu_{qcq}|$ as function of φ_w and T_c for $\nu = 0.15$ and $f_0 = 10$Hz

Thus, if we consider shear-wave incidence in an infinite medium, the maximum stresses are obtained for vertical SV-incidences. However, the relevant stress for SV-incidence is compressional, whereas that for SH-incidence is a shear stress. As the nature of the stresses is different for both shear waves, it is judicious to take into account the effects of both waves for earthquake-resistant design.

To conclude, the study of the diffraction of monochromatic plane waves by cylindrical cavities in an infinite medium provides a better understanding of the physical phenomena at stake around the structures and allows better calculation of mechanical fields under various types of incidence. For preliminary earthquake-resistant design analysis, a simplified frequency, f_0, and a peak velocity, v_0, of the expected earthquake motion at the target underground site can be obtained from seismo-tectonic information and earthquake-design regulation codes or empirical study (see [Betbeder-Matibet, 1999] and [Rathje et al., 1998]). If c_s is known, the critical radius, a_c, for which the peak stress occurs at frequency f_0 is :

$$a_c = 0.08 c_s / f_0 = 8\% \text{ of the wave length} \qquad (11)$$

Thus, from the dynamic viewpoint, it is better to design a cavity with a radius either smaller than or much larger than a_c. A response analysis of a cavity subjected to a monochromatic wave of frequency equal to the simplified frequency of the expected seismic movement can yield a good estimate of the maximum stress around the cavity during the duration of the movement.

For instance, if the fundamental frequency of the site is assumed to be $f_0 = 5$ Hz and the peak velocity is $|v_0| = 0.05$ m/s, the maximum dynamic stress around the cavity occurs for $T_c = a_c/c_s \simeq 0.02$ s.

By using the rock properties of the Kamaishi mine ($\rho = 2600$ kg/m^3, $c_s = 3000$ m/s), the peak amplitude is, by using Eq.(8) about 0.9 MPa when $a_c \simeq 24$ m. The largest dimension of an underground structure in that site should be lower or much higher than 24 m.

4 Earthquake-response analysis of unlined or lined cavity in infinite media

To understand the behavior of underground structures and their surrounding rock mass under seismic loading and to suggest an earthquake design method, it is necessary to know the properties of seismic signals at depth. For a decade, efforts have been made to develop an underground earthquake recording network, especially in Japan and in California, but the number of such recording sites and data remains small ([Nasu, 1931], [Iwasaki et al., 1977], [O'Brien and Saunier, 1980]). Since 1990, wells at Garner Valley, California, have been equipped with accelerometers to a depth of 500 meters in a granitic rock mass near and parallel to the San Jacinto Fault [Archuleta et al., 1992]. In their study of the Shin Usami tunnel, Izu Peninsula, Japan, Yamaguchi et al. [Yamaguchi and al., 1988] compared the ground motions at the tunnel entrance, inside the tunnel and in the rock mass with great overburden. Fukushima et al. [Fukushima et al., 1995] used more than 500 earthquake data recorded at depths between 100 and 950 meters. Examples of the variability of ground motions with depth are presented below, using the data from the Kamaishi Mine, in Iwate, Japan, which was recorded between 1988 and 1998 by the Japan Nuclear Cycle Research Institute (JNC). Various hydromechanical measurements were carried out in the old mine galleries at different depths. Seven accelerometers, an inflow meter, electric conductivity measurer, water sampler and strainmeter are set up from the ground surface to -615 m and three water-filled boreholes are equipped with water-pressure at -315 m [Shimizu et al., 1996]. The rock mass is mainly formed by diorite and granodiorite. About 330 earthquake motions are recorded at this site. Those studies yield that : (i) the frequency contents of a rock mass near surface and at depth are quite similar ; (ii) the motion amplitude at depth is smaller than the motion at ground surface by a factor of 2 to 10 ; (iii) at great depth, the motions measured in the underground structure and in the surrounding rock mass are similar in frequency content and amplitude — that is, the structure follows the motion of the surrounding ground ; (iv) the three horizontal and vertical directions must be taken into account for the response analysis of structure at great depth.

Theoretically, earthquake records give time-sampled values of velocity, from which the corresponding Fourier transform can be computed. If (i) at the origin $x = 0$, the incident velocity is $v_0[m]$, $m = 1, .., N$, where N is the total number of data points sampled with timestep T (the corresponding Fourier amplitude is noted $v_0[k]$, $k = 1, .., N$) ; and (ii) the hypothesis of plane-wave propagation is kept, then the velocity Fourier amplitude at point x is given by $v_0[k] \exp(i\beta_k x) = \sum_{n=0}^{\infty} \epsilon_n i^n J_n(\beta_k r) \cos(n\theta)$, with $\beta_k = \omega_k/c_s = 2\pi k/(NTc_s)$. Thus, the frequency-sampled mechanical stresses and displacements at $r = a$ can be given by using Eqs.(5) and (6) and replacing ω by $\omega_k = 2\pi k/(NT)$. Their inverse Fourier transforms correspond to the time-sampled stress component around the cavity if the surrounding medium is infinite, elastic, linear, isotropic and homogeneous.

The mechanical fields can be calculated for any wave type and incident angle. However, in general, the three components of ground motion are needed to evaluate the incident angle and the SH- and SV-components of ground motion in relation to the direction of the cavity axis. Hence, the direction of shear wave propagation has to be estimated, for example, by using the analysis of principal components of Matsuura (see [Fukushima, 1994], [Matsuura, 1981]). Then, the projections of ground motion upon the directions defined by the plane containing the cavity cross-section and the direction of S-wave propagation allow the SH- and SV-components of motion to be determined. Eqs.(5)~(6) yield the stresses and displacements around the cavity. Those operations are needed to compare numerical results and observations.

Comparison between computed and measured water pressure at the Kamaishi mine

At the Kamaishi mine, earthquake-related accelerations and dynamic pressure are available. Thus, in this section, the dynamic pressures are computed by using acceleration records obtained near the pressure-measurement device and compared to the observed values. The water pressure is measured in three water-filled (two horizontal and one 20-degree-inclined), 315-meter deep boreholes, at the Kamaishi mine. These boreholes have a diameter of 48 millimeters. The pressure transducers and a seismograph are located at the head of boreholes. The difference between the numerical and measured values of mean pressure, relative to the inclined borehole, is determined using the ground motion for earthquake 206 (magnitude 7.5, epicentral distance 217.6 km, this earthquake induced the greatest pressure variation experienced by the mine during the 1988-1998 period). The calculation method of the mean pressure in a borehole is given in Appendix B. The signal and the Fourier spectrum are shown in Fig.4, for the measured and calculated pressure at horizontal borehole KWP-1. The peak values do not occur at the same moment, but the frequency content and the amplitude are quite similar. Such correlations are obtained when the S-wave arrival time is clearly determined. Those figures show a good correlation between computed and measured results and prove the efficiency of the analytical method for underground dynamic-response of boreholes of circular cross section.
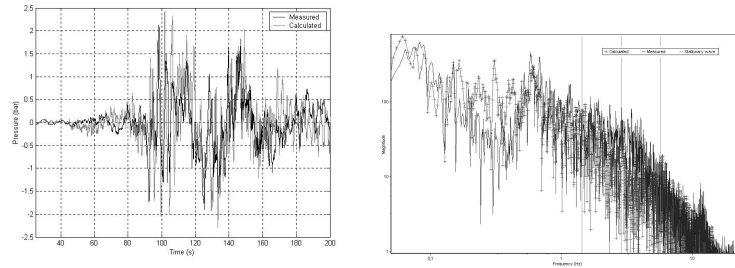

FIG. 4 – Measured and calculated pressure at borehole KWP-1 during earthquake No. 206. Left - Time series, Right - Fourier spectrum

Earthquake-response spectra for underground structures

A total of 21 earthquake motions are used to compute the normalized $SRS/(\rho c_s v_M)$-values. They were recorded from 1988 to 1998 by the Japan Nuclear Cycle Research Institute (JNC) in a 315-meter deep gallery in a granodioritic rock mass at the Kamaishi Mine in Iwate, Japan. The motions correspond to earthquakes for which the maximum accelerations, measured at a depth of 615 meters, were higher than 2 cm/s^2. Among the 21 earthquakes, the JNC considers 15 motions to have been generated by ruptures at the subduction zones (interplate earthquakes, group 1) and 6 earthquakes to have been intraplate earthquakes (group 2). Table 1 shows the number of earthquakes used for the SRS computation as a function of magnitude, provided by the Japan Meteorological Agency, and the computed mean velocity for each case. The epicentral distances range from 41 km to 460 km for group 1, and from 12 km to 53 km for group 2.

The normalized values, $SRS/(\rho c_s v_M)$, where v_M is the peak ground velocity, are computed as functions of T_c, varying from 0.0005 s to 0.02 s and magnitude M. Figure 5 shows the mean and deviation curves as functions of T_c for different magnitudes. Using the rock data from the Kamaishi

Magnitude	Group 1		Group 2	
	No	V_{mean} (cm/s)	No	V_{mean} (cm/s)
$4 < M \leq 5$	5	0.1	3	0.3
$5 < M \leq 6$	4	0.3	3	0.3
$6 < M \leq 7$	3	0.5	0	$\times$
$7 < M$	3	1.7	0	$\times$

TAB. 1 – Earthquakes used for the SRS computation

Mine, ($c_s = 3000$ m/s, $\rho = 2600$ kg/m^3) and the mean velocity values of ground motion in Table 1, the maximum SRS values increase with magnitude are about 0.05 MPa for $4 < M \leq 6$, 0.08 MPa for $6 < M \leq 7$, and 0.3 MPa for $7 < M$.
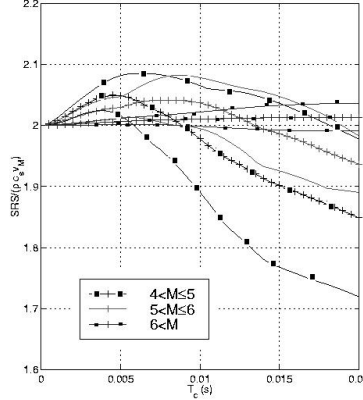

FIG. 5 – Left - Normalized spectra $SRS/\rho c_s v_M$ as functions of characteristic period T_c and magnitude M for vertical SH-incidence. Mean curve (+) and envelop curves (-)

Thus, the stress-response spectrum may be a good tool to analyze the earthquake response of deep underground structures. The SRS computation for several earthquakes seems to classify them as functions of seismological characteristics, such as the magnitude or the simplified frequency. However, data from thousands of earthquake are needed to conclude such a seismological issue, and more seismological characteristics than the only magnitude have to be taken into consideration.

Damage in mountain tunnels and numerical interpretation

To understand the failure modes in mountain tunnels during the 1995 Hyogo-ken Nanbu earthquake, the stresses induced in the lining are calculated, by using the formulae of Section 2. The vertical incident wave is assumed to be of SV-type, which can yield compressional stress in the tunnel lining ; the North-South component of the KBU signal, recorded at the Kobe University during the earthquake mentioned above, is used. This signal is recorded at a depth of 10 meters in a granitic rock site, and the peak velocity is 54 cm/s. Its simplified frequency is about 1 Hz.

The parameters suggested by Uenishi et al. [Uenishi et al., 1999] are used for the lining and the

surrounding rock mass. Thus, external radius a and internal radius b of the lining are 4.3 and 4 meters, respectively. The bulk density, the shear wave velocity and the Poisson's ratio are respectively, $\rho_l = 2200$ kg/m^3, $c_{sl} = 2700$ m/s and $\nu_l = 0.15$. Two series of parameters are used for the rock mass, as presented in Tab.2. In case 1, the rock mass is stiffer than the lining ; in case 2, the rock mass is weaker.

Case	ν_m	ρ_m(kg/m^3)	c_{sm}(m/s)
1 (Fig.6 Left)	0.25	2200	3814
2 (Fig.6Right)	0.15	2200	1907

TAB. 2 – Parameters used for the surrounding rock mass

In Figs.6(Left) and (Right), the stress path in the lining at $r = a$ and $r = b$ is presented in a Mohr-Coulomb diagram during the whole duration of the North-South component of KBU signal. The stresses are evaluated at $\theta = 45^o$ where the maximum stresses are obtained. Letters D and S correspond to dynamic and static stresses, respectively. The static stresses are calculated when considering that the overburden depth of the tunnel is $H = 300$ meters and the static stress is only due to the overburden weight, equal to $\rho_m gH$ where $g = 9.81$ m/s^2. In those figures, Coulomb failure criteria for the lining are given when the tensile strength is 3.5 MPa and three values of compressional strength, are considered, respectively R_c, 50 MPa, 100 MPa and 150 MPa. In any case, the maximal shear in the lining, τ_{max}, is greater at the internal wall than at the external wall. In case 1, for which the rock mass is stiffer than the lining, the stress path intersects the failure criteria for $Rc = 50$ MPa and $Rc = 100$ MPa at $r = b$, the total normal stress being slightly negative, whereas, in case 3, the failure does not occur. Thus, at a $\theta = 45^o$ angle to the direction of wave propagation, failure zones in the lining may appear.
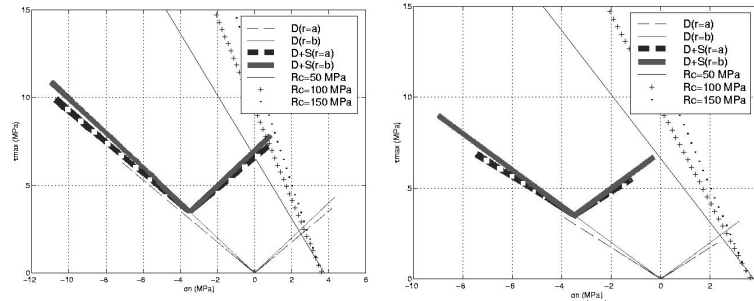

FIG. 6 – Stress path in a Mohr-Coulomb diagram during the duration of the North-South component of KBU signal at $r = a$ and $r = b$ in the lining. Left - Case 1, Right - Case 2. Letters D and S correspond to dynamic and static stresses, respectively. Coefficient R_c is the compressional strength of the lining.

5   Conclusions

A simple model of a deep cylindrical structure in an infinite medium is used to understand the physical phenomena around a gallery. To do this, actual seismic signals are introduced. The introduction of earthquake data and the differences between the computational results and the observations, such as the measurement of water pressure in a very deep borehole or the damage observation of mountain tunnels during the 1995 Hyogo-ken Nanbu earthquake, show that the proposed calculation method can yield a satisfying approximation of the observed phenomena. These methods can be used at the time of preliminary site selection or during preliminary calculations : (i) If a simplified signal frequency at a given site can be estimated (assuming that the structure is cylindrical, with circular cross-section, in an infinite medium), the value of the radius of the structure for which the stress is maximum can be determined. (ii) Applying reference earthquake motion at a given site, calculations can first be made of the stress exerted on the lining of a tunnel that is assumed to be cylindrical with circular cross-section. Thus, the mechanical parameters of the lining can then be adjusted to avoid failure. Second, verification of the stresses in the lining can be achieved with the cross-section of the actual projected structure using a finite-element method. By this way, types of support for deep structures can be proposed for a given seismotectonic context.

6   ACKNOWLEDGEMENTS

A   Dimensionless functions for a lined and unlined cavity

A cavity of radius a is considered ; it has a lining of thickness e that is in perfect contact with the surrounding medium. The internal wall of the lining (radius $b = a - e$) is a traction-free surface and $\eta = b/a = (a - e)/a$. The medium and the lining are assumed to be elastic linear, homogeneous and isotropic, and have different mechanical characteristics. The structure is subjected to an incident plane wave propagating in the medium with an angle φ_w between the propagation direction and the tunnel axis. In the following, subscripts m and l correspond to the medium and the lining, respectively, c_p and c_s are the P- and S-wave velocities, respectively, ρ is the bulk density, ν is Poisson's ratio. The dimensionless mechanical parameters are defined as :

$$\tilde{c}_p = c_{pm}/c_{pl}, \qquad \tilde{c}_s = c_{sm}/c_{sl}, \qquad \tilde{\rho} = \rho_m/\rho_l, \tag{12}$$

with the relation :

$$\tilde{c}_s = \kappa(\nu_l)\tilde{c}_p/\kappa(\nu_m) \tag{13}$$

in which the κ-function is defined by Eq.(1). If ω is the circular frequency, $\alpha = \omega/c_p$, $\beta = \omega/c_s$. Then, wave numbers $\alpha_{wm}, \beta_{wm}, \alpha_{wl}$ and β_{wl} are defined by using Eqs.(2), (3) and (4).

As examples, some dimensionless stress functions μ_{ij}^{hw} used in the paper are given for the medium and the lining, in the frequency domain.

$$\mu_{\theta\theta}^{hw} = \mu_0^w \sum_{n=0}^{\infty} \epsilon_n i^n \cos(n\theta) \times$$

$$\times \left[D_n \mathcal{E}_{21}^{(1)} + F_n \mathcal{E}_{21}^{(3)} + G_n \mathcal{E}_{22}^{(1)} + L_n \mathcal{E}_{22}^{(3)} + \frac{a}{r} \left(M_n \mathcal{E}_{23}^{(1)} + N_n \mathcal{E}_{23}^{(3)} \right) \right] \tag{14}$$

$$\mu_{\theta z}^{hw} = \mu_0^w \sum_{n=0}^{\infty} \epsilon_n i^n \sin(n\theta) \times$$

$$\times \left[-D_n \mathcal{E}_{61}^{(1)} - F_n \mathcal{E}_{61}^{(3)} + G_n \mathcal{E}_{62}^{(1)} + L_n \mathcal{E}_{62}^{(3)} - \frac{a}{r} \left(M_n \mathcal{E}_{63}^{(1)} + N_n \mathcal{E}_{63}^{(3)} \right) \right] \tag{15}$$

In the surrounding medium, $D_n = 1$ and $G_n = M_n = 0$. Tab.3 gives coefficients μ_0^w.

Coefficient	Surrounding medium		Lining	
	SV	SH	SV	SH
μ_0^w	$-\frac{2}{\beta_m^2 r^2}$	$-\frac{2}{i\beta_m^3 r^3}\frac{r}{a}$	$-\frac{2\tilde{c}_s}{\beta_l^2 r^2}$	$\frac{2\tilde{c}_s^2}{i\beta_l^3 r^3}\frac{r}{a}$

TAB. 3 – Coefficients π_0^w and μ_0^w

The dimensionless functions of the form $\mathcal{E}_{kl}^{(j)}$ are given following Mow and Pao's notation [Pao and Mow, 1973]. The $E_n^{(j)}$ functions are Bessel or Hankel functions. Superscripts $(j) = 1, 2$ are used to identify different Bessel functions, and $(j) = 3, 4$ are used to identify Hankel functions of the first and the second kinds, respectively :

$$E_n^{(1)} = J_n, \; E_n^{(2)} = Y_n, \; E_n^{(3)} = H_n^{(1)}, \; E_n^{(4)} = H_n^{(2)} \tag{16}$$

Lamé's coefficients λ and μ are used and defined, as a function of compressional and shear wave velocities c_p and c_s and bulk density ρ :

$$\lambda = \rho(c_p^2 - 2c_s^2), \qquad \mu = \rho c_s^2 \tag{17}$$

$$\mathcal{E}_{21}^{(j)} = -(n^2 + n + \frac{\beta^2 r^2}{2} - \alpha^2 r^2) E_n^{(j)}(\alpha_w r) + \alpha_w r E_{n-1}^{(j)}(\alpha_w r) \tag{18}$$

$$\mathcal{E}_{22}^{(j)} = n \left[(n+1) E_n^{(j)}(\beta_w r) - \beta_w r E_{n-1}^{(j)}(\beta_w r) \right] \tag{19}$$

$$\mathcal{E}_{23}^{(j)} = (i\gamma r) \left[-(n^2 + n) E_n^{(j)}(\beta_w r) + \beta_w r E_{n-1}^{(j)}(\beta_w r) \right] \tag{20}$$

$$\mathcal{E}_{61}^{(j)} = i\gamma r n E_n^{(j)}(\alpha_w r) \tag{21}$$

$$\mathcal{E}_{62}^{(j)} = \frac{i\gamma r}{2} \left[n E_n^{(j)}(\beta_w r) - \beta_w r E_{n-1}^{(j)}(\beta_w r) \right] \tag{22}$$

$$\mathcal{E}_{63}^{(j)} = \frac{1}{2} n (\beta_w^2 r^2 - \gamma^2 r^2) E_n^{(j)}(\beta_w r) \tag{23}$$

B Diffraction of elastic waves by a fluid inclusion

A non-viscous fluid inclusion of radius a, bulk density ρ_f and sound velocity c_f is considered in an infinite, elastic linear, homogeneous and isotropic medium. The state of the fluid is characterized by pressure, p, and fluid displacement, $\underline{u}$, which are related by the formula

$$\kappa_s p = -div\underline{u} \tag{24}$$

in which κ_s is the adiabatic compressibility coefficient of the fluid. For a non-viscous fluid of bulk density ρ_f, the pressure and the displacement verify the wave equation :

$$\Delta f = \frac{1}{c_f^2} \frac{\partial^2 f}{\partial t^2} \tag{25}$$

where c_f is the sound velocity of the fluid defined by

$$c_f = \frac{1}{\sqrt{\rho \kappa_s}} \tag{26}$$

In the frequency domain, Eq.(25) yields

$$\Delta f^* = -\alpha_f^2 f^* \tag{27}$$

where

$$\alpha_f = \omega/c_f \tag{28}$$

with ω being the circular frequency.

The bulk density, shear wave velocity and Poisson's ratio of the medium are respectively noted ρ_m, c_{sm} and ν_m. Dimensionless bulk density is defined as $\tilde{\rho} = \frac{\rho_m}{\rho_f}$. The wave numbers are defined as :

$$\beta_m = \omega/c_{sm}, \quad \alpha_f = \omega/c_f, \quad \gamma = \beta_m \cos\varphi_s, \quad \alpha_{wf} = \sqrt{\alpha_f^2 - \gamma^2} \tag{29}$$

In the frequency domain, the fluid pressure is given by the formula :

$$p(r, \theta) = \rho_m c_{sm} v_0 \mu_f^w(\varphi_w, \nu_m, \beta_m a, \beta_m r, \theta) \exp(i\gamma z) \tag{30}$$

for SH-incidence,

$$\mu_f^{sh}(\varphi_s, \nu_m, \beta_m a, \beta_m r, \theta) = -\frac{1}{i\tilde{\rho}\beta_m a} \sum_{n=0}^{\infty} \epsilon_n i^n D_n J_n(\alpha_{wf} r) \cos(n\theta) \tag{31}$$

Coefficient D_n is obtained, for each index n, by the continuity of sradial stress and pressure at $r = a$. The time variation of fluid pressure is obtained by applying the inverse Fourier transformation to formula (30).

The mean pressure p_{mean} upon the structure's cross-section at $z = 0$ is calculated. If the shear wave propagation is considered, it can be shown that only the SH component can induce a non-zero mean pressure. In the frequency domain, using Eq.(30), p_{mean} can be obtained for SH-incidence by :

$$p_{mean} = -\rho_m c_{sm} v_0 D_0 \frac{1}{i\tilde{\rho}\beta_m a} \tag{32}$$

with the assumption that $\alpha_{wf} a \ll 1$.

Références

Archuleta, R., Seale, S., Sangas, P., Baker, L., and Swain, S., 1992, "Garner Valley downhole array of accelerometers : instrumentation and preliminary data analysis," *Bull. Seism. Soc. Am.*, vol. 82, pp. 1592–1621.

Asakura, T., Kojima, Y., Kobayashi, M., Sato, Y., Yashiro, K., and Shiba, Y., 1998, "Damage to mountain tunnels by earthquake and its mechanism (in Japanese)," *Proc. 10th Annual National Symp. Rock Mech.*, Japan, pp. 497–502.

Betbeder-Matibet, J., 1999, "L'atténuation des mouvements sismiques en profondeur - in depth attenuation of seismic ground motions (in French)," *Génie Parasismique et Réponse Dynamique des Ouvrages. 5ème Colloque National AFPS*, pp. 51–56.

Clure, C. M., 1982, "Damage to underground structures during earthquakes," *Proc. workshop on seismic performance of underground facilities*, eds. W. V. Oz and M. Yannakakis, no. DP-1623 in All ACM Conferences, E.I. du Pont de Nemour & Co, Savannah river lab., Aiken S.C., pp. 43–74.

Dowding, C., 1979, "Earthquake stability of rock tunnels," *Tunnels and Tunnelling*, vol. 11 (5), pp. 15–20.

Dowding, C. and Rozen, A., 1978, "Comparative studies of earthquake motions," *J. Geotech.Eng. Div., A.S.C.E.*, vol. 104 (GT-2), pp. 175–191.

Duke, C. and Leeds, D., 1959, "Effects of earthquakes on tunnels," *RAND Protective Construction Symp.*, vol. 2, Paper 1762, p. 27.

Fukushima, Y., 1994, "Empirical prediction for strong ground motion reflected on theoretical backgrounds of source and propagation of seismic wave," Technical report ORI 93-07, Shimizu Corp.

Fukushima, Y., Gariel, J.-C., and R.Tanaka, 1995, "Site-dependent attenuation relations of seismic motion parameters at depth using borehole data," *Bull. of the Seismogical Soc. of Am.*, vol. 85 (6), pp. 1790–1804.

Iwasaki, T., Wakabayashi, S., and Tatsuoka, F., 1977, "Characteristics of underground seismic motions at four sites around Tokyo Bay," *Wind and Seismic Effects*, ed. L. H.S., US Dpt. Commerce, Washington DC.

Kurose, A., 2000, *Earthquake-related effects on underground structures (in French, summary in English)*, PhD dissertation, Ecole Polytechnique, Palaiseau, France.

Martin, G. and Godefroy, P., 1991, "Comportement des massifs rocheux et de ouvrages souterrains et perturbations hydrogéologiques sous actions sismiques (in French)," Technical report no.620 RP BRG 91-005, ANDRA.

Matsuura, S., 1981, "Three-dimensional expression of seismic particle motions by the trajectory ellipsoid and its application to the seismic data observed in the Kanto District, Japan," *J. Phys. Earth*, vol. 29, pp. 221.

Nasu, S., 1931, "Comparative studies of earthquake motions above-ground and in a tunnel (part 1)," *Bull. Earthquake Research Institute, Japan*, vol. 9(4), pp. 454–472.

Nogami, T. and Zhu, J., 1994, "Transient response of finitely long cylindrical cavity with arbitrary cross-section," *Soil Dyn. and Earthquake Eng.*, vol. 13, pp. 31–43.

O'Brien, L. and Saunier, J., 1980, "Comparison of predicted and observed subsurface-surface seismic spectral ratios," Contrat EY-76-C-08-0624, Rep. Computer Sci. Corp. for Dpt. Energy.

Owen, G. and Scholl, R., 1979, "Earthquake engineering of large underground structures," Tech. Rep. FHWA/RD-80/195, FHWA, San Francisco, California.

Pao, Y.-H. and Mow, C.-C., 1973, *Diffraction of Elastic Waves and Dynamic Stress Concentrations*, Crane, Russak and Co. Inc., ISBN 0-8448-0155-0.

Power, M., Rosidi, D., and Kaneshiro, J., 1998, "Seismic vulnerability of tunnels and underground structures revisited," *North American Tunneling '98*, Balkema, Rotterdam.

Rathje, E., Abrahamson, N., and Bray, J., 1998, "Simplified frequency content estimates of earthquake ground motion with a single parameter," *J. Geotech. and Geoenviron. Eng*, vol. 124 (2), pp. 150–159.

Sakurai, S., 1995, "Damage to tunnels due to the earthquake and relation to location of active faults (in Japanese)," *Special Issue on the 1995 Hanshin Awaji Great Earthquake*, Construction Engineering Research Institute Foundation.

Sharma, S. and W.R., J., 1991, "Underground opening damage from earthquakes," *Engineering Geology*, vol. 30, pp. 263–276.

Shimizu, I., Osawa, H., Seo, T., Yasuike, S., and Sasaki, S., 1996, "Earthquake-related ground motion and groundwater pressure change at the Kamaishi Mine," *Eng. Geol.*, vol. 43, pp. 107–118.

Uenishi, K., Mizoguchi, S., and Sakurai, S., 1999, "Theoretical study on earthquake-induced damage to a tunnel in the mountainous region," *Special Issue on the 1995 Hanshin-Awaji Great Earthquake*, Construction Engineering Research Institute Foundation.

Yamaguchi, Y. and al., 1988, "Earthquake observations in deep rock," Tech. rep., Technical Research Inst. Hazama Gumi Ltd.